

Neutrino-nucleus cross sections in ^{12}C and ^{40}Ar with KDAR neutrinos

F. Akbar,¹ M. Sajjad Athar,^{1,*} and S. K. Singh¹

¹*Department of Physics, Aligarh Muslim University, Aligarh-202002, India*

High intensity monoenergetic muon neutrinos of energy 236 MeV from kaon decay at rest (KDAR) at the medium energy proton accelerator facilities like J-PARC and Fermilab are proposed to be used for making precision measurements of neutrino-nucleus cross sections in ^{12}C and ^{40}Ar and perform neutrino oscillation experiments in $\nu_\mu \rightarrow \nu_\mu$ and $\nu_\mu \rightarrow \nu_e$ modes. In view of these developments, we study the theoretical uncertainties arising due to the nuclear medium effects in the neutrino-nucleus cross sections as well as in the angular and energy distributions of the charged leptons produced in the charged current (CC) induced reactions by ν_μ and ν_e in ^{12}C and ^{40}Ar in the energy region of $E_{\nu_e(\nu_\mu)} < 300$ MeV. The calculations have been done in a microscopic model using the local density approximation which takes into account the nuclear effects due to the Fermi motion, binding energy and long range correlations. The results are compared with the other calculations available in the literature.

PACS numbers: 12.15.-y,13.15+g,24.10Cn,25.30Pt

arXiv:1708.00321v1 [nucl-th] 29 Jul 2017

* sajathar@gmail.com

I. INTRODUCTION

The two body leptonic decay mode of the charged kaon decay-at-rest (KDAR) i.e. $K^+ \rightarrow \mu^+\nu_\mu$, B.R. $63.55 \pm 1.1\%$ [1] provides a unique and important source of monoenergetic muon neutrinos of energy 236 MeV. These neutrinos may be used to make high precision measurements of neutrino-nucleus cross sections for the charged current (CC) induced weak quasielastic (QE) production of muons from the various nuclear targets. The high precision neutrino-nucleus cross section measured with the well defined monoenergetic beam of muon neutrinos may serve as benchmark for validating many theoretical models currently being used to describe the nuclear medium effects in QE reactions [2, 3] relevant for the analysis of present day neutrino experiments in the low energy region of a few hundred MeVs [4–21].

These KDAR neutrinos are proposed to be used as a probe to study the new neutrino oscillation modes to sterile neutrinos i.e. $\nu_\mu \rightarrow \nu_s$ by performing the oscillation experiments in $\nu_\mu \rightarrow \nu_\mu$ disappearance mode and studying the CC interactions of ν_μ with nuclei and/or performing the oscillation experiments in $\nu_\mu \rightarrow \nu_e$ appearance mode and studying the CC interaction of ν_e with nuclei [15–21]. In the $\nu_\mu \rightarrow \nu_\mu$ disappearance mode, ν_μ from the three body $K\mu_3$ decays of charged kaons i.e. $K^+ \rightarrow \mu^+\pi^0\nu_\mu$ having continuous energy spectrum with the end point energy of 215 MeV constitute the major source of background while in the $\nu_\mu \rightarrow \nu_e$ appearance mode, ν_e from the Ke_3 decay mode of charged kaons i.e. $K^+ \rightarrow e^+\pi^0\nu_e$, having continuous energy spectrum with end point energy of 228 MeV constitute the major source of background. The background in both the channels from the decay in flight (DIF) neutrinos from pions, kaons and other mesons corresponds to higher energies. With sufficiently improved energy resolution for the detection of the final muon and the electron produced respectively in the CC weak interaction of ν_μ and ν_e with matter, the background events can be well separated in energy from the signal events for the oscillation experiments corresponding to $E_{\nu_\mu(\nu_e)} = 236$ MeV. Moreover, it has been recently suggested [22] that the observation of CC induced QE events with the monoenergetic neutrinos can also provide information about the dark matter which annihilates in its interaction with the solar matter in the center of the Sun into quark-antiquark pairs and produces the charged kaons through the hadronization process. The monoenergetic muon neutrinos produced by these charged kaons through the $K\mu_2$ decays can be identified by comparing the on-source and off-source event rates in the terrestrial detectors provided the background events for $E_\nu \sim 236$ MeV are well under control in the ν -oscillation experiments proposed with the KDAR neutrinos.

The feasibility of such experiments with high intensity KDAR neutrinos requires an accelerator facility capable of producing K^+ mesons with a very high yield. The 3 GeV proton accelerator facility at the J-PARC MLF facility in Tokai, Japan [15–19] and the 8 GeV proton accelerator facility at the BNB source facility at the Fermilab, USA [19–21] have the sufficient energy and power to produce high intensity charged kaons through the primary and/or secondary interactions of protons with the nuclear targets which would be stopped in the surrounding material and their decay would give intense beam of ν_μ . At the J-PARC facility the neutrino oscillation experiments in the appearance mode i.e. $\nu_\mu \rightarrow \nu_e$ as well as in the disappearance mode i.e. $\nu_\mu \rightarrow \nu_\mu$ have been proposed respectively, through the JSNS experiment by the Japanese group [15–17], and the KPipe experiment by the MIT-Columbia group [18–20] using the liquid scintillator detector with active detector mass of 17 tons and 684 tons, respectively. At the Fermilab facility a neutrino oscillation experiment in the appearance mode i.e. $\nu_\mu \rightarrow \nu_e$ has been proposed with 2 kton LArTPC detector [20, 21].

One of the major sources of systematic errors in these experiments is due to the ν_μ flux arising from the uncertainty in the K^+ production yields in the proton-nucleus interaction predicted by the hadronic models for the kaon production and could be as large as 75% [18, 19, 23, 24]. The other source of systematic errors is due to the uncertainty in the $\nu_\mu(\nu_e)$ -nucleus cross sections for $E_{\nu_\mu(\nu_e)} = 236$ MeV arising due to the nuclear medium effects [2, 3] and is the subject of the present work.

The present simulation studies [18–20], for estimating the neutrino oscillation parameters, use the neutrino nucleus cross sections for the KDAR neutrinos on ^{12}C and ^{40}Ar as predicted by the NuWro generator [25] which are reported to be about 25% smaller than the predictions by the GENIE Monte Carlo generator [26] and the results of Martini et al. [27, 28]. In the low energy region, the short range correlations and the meson exchange currents (MEC) are not expected to play an important role [29–31], but the effects of Pauli blocking, Fermi motion and the long range RPA correlations are found to be quite important. This has been shown by many theoretical attempts [32–44] made to explain the ν_μ - ^{12}C cross section measured in the LSND experiment [45–47] with the pion decay in flight (DIF) muon neutrinos in the energy region of $E_{\nu_\mu} < 320$ MeV with $\langle E_{\nu_\mu} \rangle = 150$ MeV. These effects could therefore be very important in the energy region of KDAR neutrinos.

In view of the recent interest in the proposed neutrino oscillation experiments in $\nu_\mu \rightarrow \nu_\mu$ and $\nu_\mu \rightarrow \nu_e$ mode with liquid scintillator (LS) and LArTPC detectors and the search of sterile neutrinos through the $\nu_\mu \rightarrow \nu_s$ mode; it is topical to study the uncertainties in the $\nu_\mu(\nu_e)$ -nucleus cross sections in the low energy region relevant for the monoenergetic KDAR neutrinos. In this paper, we have studied the uncertainties in the neutrino-nucleus cross sections for the QE processes induced by the weak charged current interaction in $\nu_\mu(\nu_e)$ scattering from ^{12}C and ^{40}Ar nuclei relevant for the KDAR neutrinos with $E_{\nu_\mu} \leq 300$ MeV in a nuclear model using the local density approximation

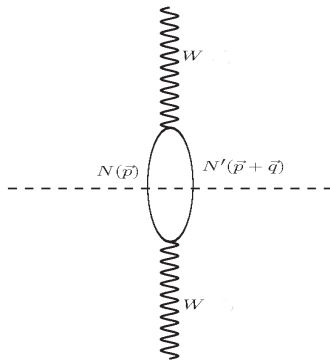


FIG. 1. Diagrammatic representation of the particle - hole(p-h) excitation induced by W boson in the large mass limit of intermediate vector boson($M_W \rightarrow \infty$).

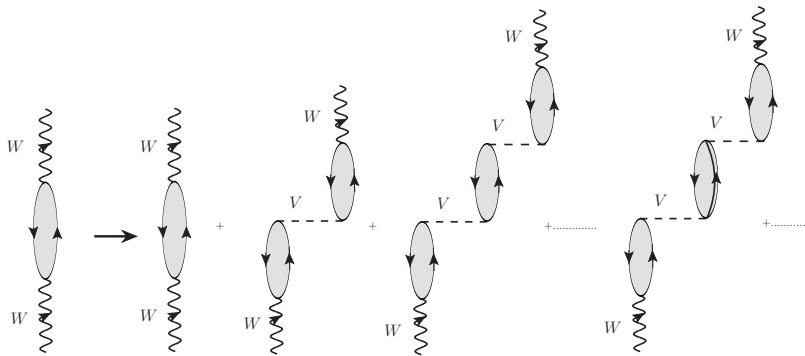


FIG. 2. RPA effects in the 1p1h contribution to the W self energy, where particle-hole, Δ -hole, Δ - Δ , etc. excitations contribute.

which takes into account the effects of nuclear medium arising due to the Pauli Blocking, Fermi motion and the long range RPA correlations. The model has been used by us earlier to calculate quite satisfactorily the low energy neutrino cross sections relevant for the supernova, Michel and pion decay in flight(DIF) neutrino spectra [48–51]. We report the results on the energy dependence of the total cross section $\sigma(E_\nu)$ for $E_\nu < 300\text{MeV}$, and the angular distributions ($\frac{d\sigma}{d\cos\theta_l}$) and the kinetic energy distributions ($\frac{d\sigma}{dT_l}$) for the electron and the muon produced in the CCQE reactions induced by ν_e and ν_μ at $E_\nu = 236\text{ MeV}$ in ^{12}C and ^{40}Ar and compare these results with the other theoretical calculations available in the literature.

II. FORMALISM

The reaction for the CC neutrino interaction with a nucleus is given by

$$\nu_l + {}^A_Z X \rightarrow l^- + {}^A_{Z+1} Y \quad (l = e, \mu) \quad (1)$$

for which the basic process is

$$\nu_l(k) + n(p) \rightarrow l^-(k') + p(p'). \quad (2)$$

${}^A_Z X({}^A_{Z+1} Y)$ is the initial(final) nucleus, and k, k' are the four momenta of the incoming and outgoing lepton and p, p' are the four momenta of the initial and final nucleon, respectively. The invariant matrix element given in Eq.(2) is written as

$$\mathcal{M} = \frac{G_F}{\sqrt{2}} \cos\theta_c l_\mu J^\mu \quad (3)$$

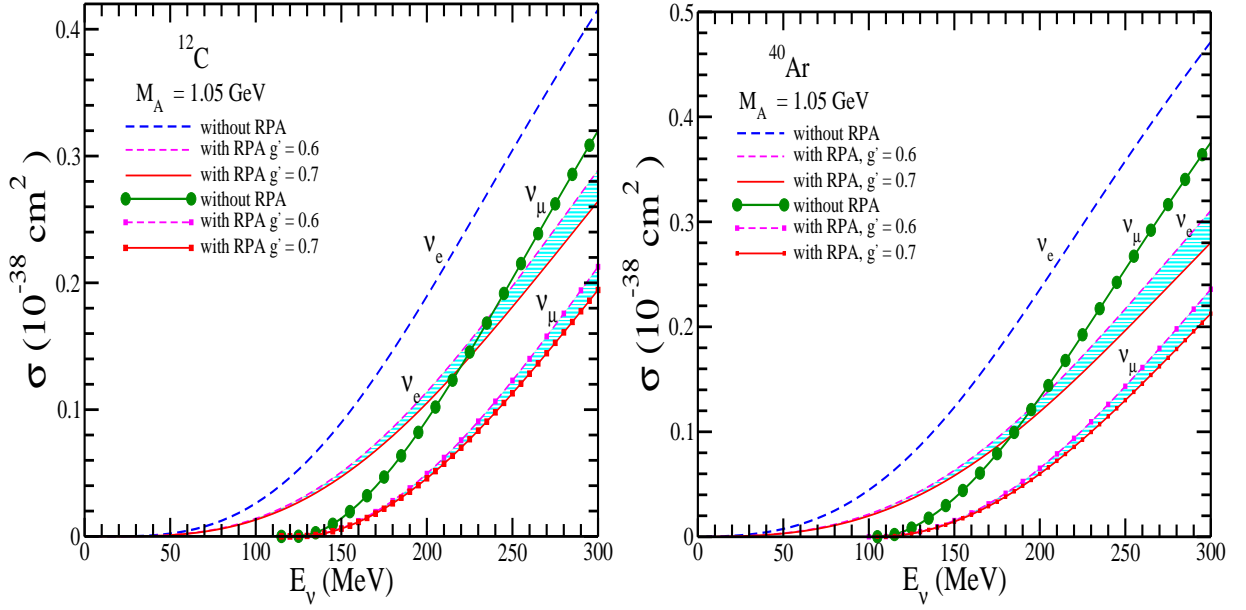


FIG. 3. σ vs E_{ν_l} , for $\nu_l (l = e^-, \mu^-)$ induced scattering on ^{12}C (left panel) and ^{40}Ar (right panel) nuclear targets. The dashed line (line with circles) represents $\nu_e (\nu_\mu)$ cross section obtained in the LFGM without RPA effects, while the bands upper (lower) represents $\nu_e (\nu_\mu)$ cross section with RPA. The bands correspond to the variation of g' in the range of 0.6-0.7.

where G_F is the Fermi coupling constant ($=1.16639 \times 10^{-5} \text{ GeV}^{-2}$), $\theta_c (= 13.1^\circ)$ is the Cabibbo angle. The leptonic weak current is given by

$$l_\mu = \bar{u}(k') \gamma_\mu (1 - \gamma_5) u(k), \quad (4)$$

J^μ is the hadronic current given by

$$J^\mu = \bar{u}(p') \Gamma^\mu u(p), \quad (5)$$

with

$$\Gamma^\mu = F_1^V(Q^2) \gamma^\mu + F_2^V(Q^2) i \sigma^{\mu\nu} \frac{q_\nu}{2M} + F_A(Q^2) \gamma^\mu \gamma^5 + F_P(Q^2) \frac{q^\mu}{M} \gamma^5, \quad (6)$$

$Q^2 (= -q^2) \geq 0$ is the four momentum transfer square and M is the nucleon mass. $F_{1,2}^V(Q^2)$ are the isovector vector form factors and $F_A(Q^2)$, $F_P(Q^2)$ are the axial and pseudoscalar form factors, respectively. We have not considered the contribution from the second class currents.

The hadronic current contains isovector vector form factors $F_{1,2}^V(Q^2)$ of the nucleons, which are given as

$$F_{1,2}^V(Q^2) = F_{1,2}^p(Q^2) - F_{1,2}^n(Q^2) \quad (7)$$

where $F_1^{p(n)}(Q^2)$ and $F_2^{p(n)}(Q^2)$ are the Dirac and Pauli form factors of proton (neutron) which in turn are expressed in terms of the experimentally determined Sachs's electric $G_E^{p,n}(Q^2)$ and magnetic $G_M^{p,n}(Q^2)$ form factors as

$$F_1^{p,n}(Q^2) = \left(1 + \frac{Q^2}{4M^2}\right)^{-1} \left[G_E^{p,n}(Q^2) + \frac{Q^2}{4M^2} G_M^{p,n}(Q^2) \right] \quad (8)$$

$$F_2^{p,n}(Q^2) = \left(1 + \frac{Q^2}{4M^2}\right)^{-1} \left[G_M^{p,n}(Q^2) - G_E^{p,n}(Q^2) \right] \quad (9)$$

$G_E^{p,n}(Q^2)$ and $G_M^{p,n}(Q^2)$ are the electric and magnetic Sachs form factors and for the numerical calculations we have used the parameterization of Bradford et al. [52].

The isovector axial form factor is obtained from the quasielastic neutrino and antineutrino scattering as well as from the pion electroproduction data and is parameterized as

$$F_A(Q^2) = F_A(0) \left[1 + \frac{Q^2}{M_A^2} \right]^{-2}; \quad F_A(0) = -1.267. \quad (10)$$

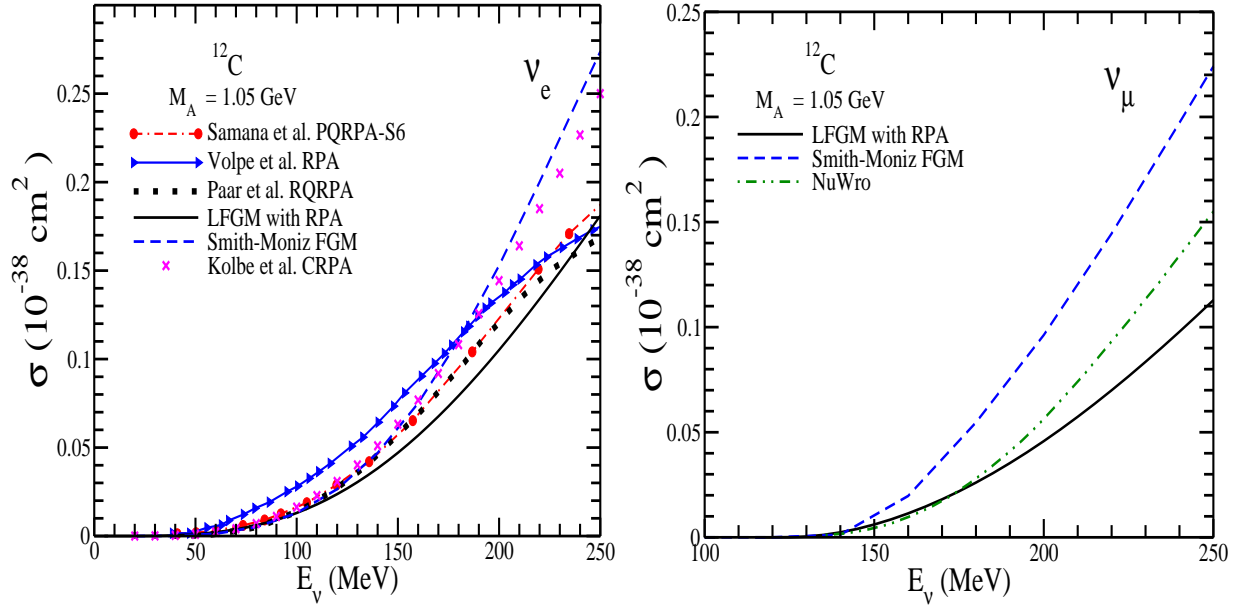


FIG. 4. σ vs E_{ν_i} , for ν_e (left panel) and ν_μ (right panel) CCQE scattering cross sections on ^{12}C in the LFGM model with RPA effect(solid line), the results of NuWro event generator taken from Ref. [20] (dashed double-dotted line), Volpe et al. [36] in RPA (triangle right), Kolbe et al. [38] in CRPA (cross), Paar et al. [42] in RQRPA (dotted line), Samana et al. [66] in PQRPA (circle), and Smith and Moniz [67] in RFGM (dashed line).

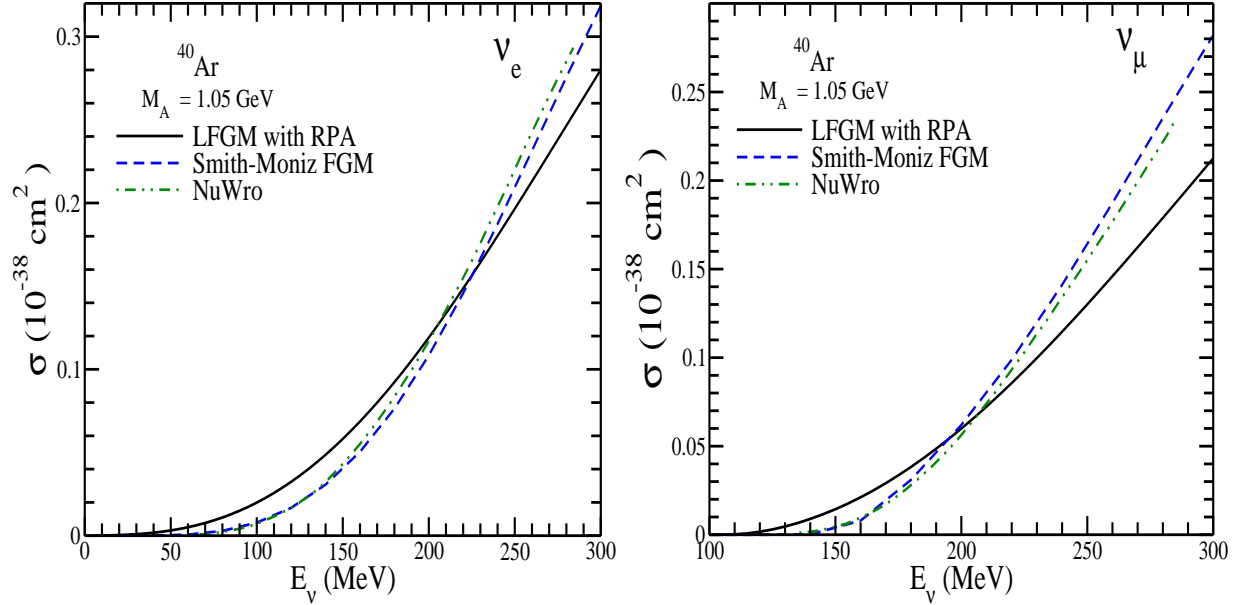


FIG. 5. σ vs E_{ν_i} , for ν_e (left panel) and ν_μ (right panel) on ^{40}Ar in the LFGM model with RPA effect(solid line), the results of NuWro generator taken from Ref. [20] (dashed - double dotted), and Smith and Moniz in RFGM [26, 67] (dashed line).

The pseudoscalar form factor $F_P(Q^2)$ is dominated by the pion pole and is given in terms of the axial vector form factor $F_A(Q^2)$ using the Goldberger-Treiman(GT) relation [53]:

$$F_P(Q^2) = \frac{2M^2 F_A(Q^2)}{m_\pi^2 + Q^2}. \quad (11)$$

The differential cross section corresponding to Eq. 2 is given by

$$\sigma_0(\mathbf{q}^2, \mathbf{k}', \mathbf{p}) = \frac{1}{4\pi} \frac{k^2}{E_\nu E_l} \frac{M^2}{E_n E_p} \bar{\Sigma} \Sigma |\mathcal{M}^2| \delta(q_0 + E_n - E_p), \quad (12)$$

where $q_0 = E_{\nu_l} - E_l$, $E_n = \sqrt{|\mathbf{p}|^2 + M_n^2}$ and $E_p = \sqrt{|\mathbf{p} + \mathbf{q}|^2 + M_p^2}$. The matrix element square is obtained by using Eq.(3) and is given by

$$|\mathcal{M}|^2 = \frac{G_F^2}{2} L_{\mu\nu} J^{\mu\nu}. \quad (13)$$

In Eq.(13), $L_{\mu\nu}$ is the leptonic tensor calculated to be

$$L_{\mu\nu} = \bar{\Sigma} \Sigma l_\mu^\dagger l_\nu = L_{\mu\nu}^S - i L_{\mu\nu}^A, \quad \text{with} \quad (14)$$

$$L_{\mu\nu}^S = 8 [k_\mu k'_\nu + k'_\mu k_\nu - g_{\mu\nu} k \cdot k'] \quad \text{and}$$

$$L_{\mu\nu}^A = 8 \epsilon_{\mu\nu\alpha\beta} k'^\alpha k^\beta, \quad (15)$$

The hadronic tensor $J^{\mu\nu}$ given by:

$$J^{\mu\nu} = \bar{\Sigma} \Sigma J^{\mu\dagger} J^\nu, \quad (16)$$

where J^μ defined in Eq.(5) with Eqs.(7), (10) and (11) has been used for the numerical calculations. The detailed expression for the hadronic tensor $J^{\mu\nu}$ is given in Ref. [54].

When the processes given by Eq. (2) take place in a nucleus, various nuclear medium effects like Pauli blocking, Fermi motion, binding energy corrections and nucleon correlations, etc. come into play. Moreover, the charged lepton produced in the final state moves in the Coulomb field of the residual nucleus and which affects its energy and momenta. We have taken into account these effects which are briefly discussed below:

1. In the standard treatment of the Fermi Gas Model applied to neutrino reactions the quantum states of the nucleons inside the nucleus are filled up to a Fermi momentum p_F , given by $p_F = [3\pi^2\rho]^{\frac{1}{3}}$, where ρ is the density of the nucleus. In a nuclear reaction, the momentum of the initial nucleon p is therefore constrained to be $p < p_F$ and $p' (= |\mathbf{p} + \mathbf{q}|) > p'_F$, where p_F is the Fermi momentum of the initial nucleon target in the Fermi sea, and p'_F is the Fermi momentum of the outgoing nucleon. The total energies of the initial(i) and final(f) nucleons are $E_i = \sqrt{|\mathbf{p}|^2 + M_i^2}$ and $E_f = \sqrt{|\mathbf{p} + \mathbf{q}|^2 + M_f^2}$. In this model the Fermi momentum and energy are constrained to be determined by the nuclear density which is constant.

In the local Fermi gas model(LFGM), the Fermi momenta of the initial and final nucleons are not constant but depend on the interaction point \vec{r} and are given by $p_{F_n}(r)$ and $p_{F_p}(r)$ for neutron and proton, respectively, where $p_{F_n}(r) = [3\pi^2\rho_n(r)]^{\frac{1}{3}}$ and $p_{F_p}(r) = [3\pi^2\rho_p(r)]^{\frac{1}{3}}$, $\rho_n(r)$ and $\rho_p(r)$ being the neutron and proton nuclear densities, respectively. We use the proton density $\rho_p(r) = \frac{Z}{A}\rho(r)$ and neutron density given by $\rho_n(r) = \frac{A-Z}{A}\rho(r)$, where $\rho(r)$ is determined experimentally by the electron-nucleus scattering experiments [55]. We use modified harmonic oscillator(MHO) density

$$\rho(r) = \rho(0) \left[1 + a \left(\frac{r}{R} \right)^2 \exp \left[- \left(\frac{r}{R} \right)^2 \right] \right] \quad (17)$$

for ^{12}C and 2-parameter Fermi density(2pF)

$$\rho(r) = \frac{\rho(0)}{[1 + \exp(\frac{r-R}{a})]} \quad (18)$$

for ^{40}Ar with R and a as the density parameters and the parameters are taken from the Refs. [55, 56]. In Table-3, we show the nuclear density and other parameters needed for the numerical calculations in this paper. In the local density approximation(LDA), the cross section(σ) for the ν_l scattering from a nucleon moving in the nucleus with a momentum \mathbf{p} is given by [57]:

$$\sigma(q^2, k') = \int 2d\mathbf{r}d\mathbf{p} \frac{1}{(2\pi)^3} n_n(\mathbf{p}(\mathbf{r})) [1 - n_p(\mathbf{p}(\mathbf{r}) + \mathbf{q}(\mathbf{r}))] \sigma_0(\mathbf{q}^2, \mathbf{k}', \mathbf{p}), \quad (19)$$

where σ_0 is given by Eq.12. In the above expression, $n_n(\mathbf{p}(\mathbf{r}))$ and $n_p(\mathbf{p}(\mathbf{r}) + \mathbf{q}(\mathbf{r}))$ represent the occupation numbers for the neutron and proton respectively i.e. at a given position \mathbf{r} , $n_n(\mathbf{p}(\mathbf{r}))=1$ for $p \leq p_{F_n}(r)$, and 0 otherwise, and $n_p(\mathbf{p}(\mathbf{r}) + \mathbf{q}(\mathbf{r}))=1$ for $|\mathbf{p}(\mathbf{r}) + \mathbf{q}(\mathbf{r})| \geq p_{F_p}(r)$, and 0 otherwise.

Instead of using Eqs. 12 and 19, we use the methods of many body field theory [58], where the reaction cross section for the process $\nu_l + n \rightarrow l^- + p$ in a nuclear medium is given in terms of the imaginary part of the Lindhard function $U_N(q_0, \vec{q})$ corresponding to the p-h excitation diagram shown in Fig.1 [57]. This imaginary part $U_N(q_0, \vec{q})$ is obtained by cutting the W self energy diagram along the horizontal line(Fig. 1) and applying the Cutkowsky rules [59]. This is equivalent to replacing the expression

$$\int \frac{d\mathbf{p}}{(2\pi)^3} n_n(\mathbf{p}) [1 - n_p(\mathbf{p} + \mathbf{q})] \frac{M_n M_p}{E_n(\mathbf{p}) E_p(\mathbf{p} + \mathbf{q})} \delta[q_0 + E_n - E_p] \quad (20)$$

occurring in Eq.(19) by $-(1/\pi)\text{Im}U_N(q_0, \vec{q})$, where

$$U_N(q_0, \mathbf{q}) = \int \frac{d\mathbf{p}}{(2\pi)^3} \frac{M_n M_p}{E_n(\mathbf{p}) E_p(\mathbf{p} + \mathbf{q})} \frac{n_n(\mathbf{p}) [1 - n_p(\mathbf{p} + \mathbf{q})]}{q_0 + E_n(\mathbf{p}) - E_p(\mathbf{p} + \mathbf{q}) + i\epsilon}. \quad (21)$$

The imaginary part of the Lindhard function is calculated to be [57]:

$$\text{Im} U_N(q_0, \mathbf{q}) = -\frac{1}{2\pi} \frac{M_p M_n}{|\mathbf{q}|} [E_{F_1} - A] \quad (22)$$

for $q^2 < 0, E_{F_2} - q_0 < E_{F_1}$ and $\frac{-q_0 + |\mathbf{q}| \sqrt{1 - \frac{4M^2}{q^2}}}{2} < E_{F_1}$,
otherwise $\text{Im} U_N = 0$.

In the above expression $E_{F_{1(2)}} = \sqrt{p_{F_{n(p)}}^2 + M_{n(p)}^2}$, and

$$A = \text{Max} \left[M_n, E_{F_2} - q_0, \frac{-q_0 + |\mathbf{q}| \sqrt{1 - \frac{4M^2}{q^2}}}{2} \right].$$

2. When the reaction $\nu_l + n \rightarrow l^- + p$ takes place in the nucleus, the first consideration is the Q value which inhibits the reaction in the nucleus. The experimental Q values corresponding to the g.s. \rightarrow g.s. transition are given in Table-I for the two nuclei. We also introduce $Q_F(r) = E_{F_2}(r) - E_{F_1}(r)$ to take into account the difference in the Fermi levels of the initial and final nuclei, which results in an effective value of $Q = Q - Q_F(r)$ to be used in the local Fermi Gas model. These considerations imply that q_0 should be modified to $q_0^{\text{eff}}(r) = q_0 - (Q - Q_F(r))$ in the calculation of the Lindhard function in Eq.22.
3. In the charged current reaction, the energy and momentum of the outgoing charged lepton are modified due to the Coulomb interaction with the final nucleus. The Coulomb distortion effect on the outgoing lepton has been taken into account in an effective momentum approximation(EMA) [60-63] in which the lepton momentum and energy are modified by replacing E_l by $E_l + V_c(r)$. The form of the Coulomb potential $V_c(r)$ considered here is:

$$V_c(r) = -\alpha 4\pi \left(\frac{1}{r} \int_0^r \frac{\rho_p(r')}{Z} r'^2 dr' + \int_r^\infty \frac{\rho_p(r')}{Z} r' dr' \right), \quad (23)$$

where α is fine structure constant and $\rho_p(r)$ is the proton density of the final nucleus.

Incorporation of these considerations results in the modification of the argument of the Lindhard function (Eq.22), i.e.

$$\text{Im}U_N(q_0, \mathbf{q}) \longrightarrow \text{Im}U_N(q_0^{\text{eff}}(r) - V_c(r), \mathbf{q}).$$

With the inclusion of these nuclear effects, the cross section $\sigma(E_\nu)$ is written as

$$\sigma(E_\nu) = -2G_F^2 \cos^2 \theta_c \int_{r_{\min}}^{r_{\max}} r^2 dr \int_{k'_{\min}}^{k'_{\max}} k' dk' \int_{Q_{\min}^2}^{Q_{\max}^2} dQ^2 \frac{1}{E_{\nu_l}^2 E_l} L_{\mu\nu} J^{\mu\nu} \text{Im}U_N(q_0^{\text{eff}}(r) - V_c(r), \mathbf{q}). \quad (24)$$

We must point out that in the above expression the outgoing lepton momentum and energy are r -dependent i.e. $k' = k'(r)$ and $E_l = E_l(r)$, and only in the asymptotic limit ($r \rightarrow \infty$) they become independent of r . With the incorporation of the Coulomb effect, $E_l(r)$ is modified to $E_l(r) + V_c(r)$, and $|\vec{k}'(r)| = \sqrt{(E_l(r) + V_c(r))^2 - m_l^2}$. Accordingly the energy transfer q_0 modifies to $q_0^{\text{eff}}(r) = q_0^{\text{eff}}(r) - V_c(r)$, and the three momentum transfer \vec{q} modifies to $\vec{q}(r) = \vec{k} - \vec{k}'(r)$.

Nucleus	Q-Value(ν) (MeV)	R_p (fm)	R_n (fm)	a (fm)*
^{12}C	17.84	1.69	1.692	1.082(MHO)
^{40}Ar	3.64	3.47	3.64	0.569(2pF)

TABLE I. Fermi momentum and Q-value of the reaction for ^{12}C and ^{40}Ar nuclear targets. Last three columns are the parameters for MHO and 2pF densities [41, 55, 56]. * is dimensionless for the MHO density.

4. In the nucleus the strength of the electroweak couplings may change from their free nucleon values due to the presence of strongly interacting nucleons. Conservation of vector current (CVC) forbids any change in the charge coupling while the magnetic and the axial vector couplings are likely to change from their free nucleon values. There exists considerable work in understanding the quenching of magnetic moment and axial charge in nuclei due to nucleon-nucleon correlations. In our approach these are reflected in the modification of nuclear response in longitudinal and transverse channels leading to some reduction. We calculate this reduction in the vector-axial(VA) and axial-axial(AA) response functions due to the long range nucleon-nucleon correlations treated in the random phase approximation(RPA), which has been diagrammatically shown in Fig.(2).

The weak nucleon current described by Eq.(5) gives in the non-relativistic limit, terms like $F_A \vec{\sigma} \tau_+$ and $iF_2^V \frac{\vec{\sigma} \times \vec{q}}{2M} \tau_+$ which generate spin-isospin transitions in nuclei. While the term $iF_2^V \frac{\vec{\sigma} \times \vec{q}}{2M} \tau_+$ couples with the transverse excitations, the term $F_A \vec{\sigma} \tau_+$ couples with the transverse as well as longitudinal channels. These channels produce different RPA responses in the longitudinal and transverse channels due to the different NN potential in these channels when the diagrams of Fig.(2) are summed up. As a consequence a term proportional to $F_A^2 \delta_{ij}$ in J^{ij} is replaced by J_{RPA}^{ij} as [54]:

$$J^{ij} \rightarrow J_{RPA}^{ij} = F_A^2 Im U_N \left[\frac{\hat{\mathbf{q}}_i \hat{\mathbf{q}}_j}{1 - U_N V_l} + \frac{\delta_{ij} - \hat{\mathbf{q}}_i \hat{\mathbf{q}}_j}{1 - U_N V_t} \right], \quad (25)$$

where the first and second terms show the modification in J^{ij} in longitudinal and transverse channels. In Eq.(25), V_l and V_t are the longitudinal and transverse parts of the nucleon-nucleon potential calculated using π and ρ exchanges and are given by

$$V_l(q) = \frac{f^2}{m_\pi^2} \left[\frac{q^2}{-q^2 + m_\pi^2} \left(\frac{\Lambda_\pi^2 - m_\pi^2}{\Lambda_\pi^2 - q^2} \right)^2 + g' \right],$$

$$V_t(q) = \frac{f^2}{m_\pi^2} \left[\frac{q^2}{-q^2 + m_\rho^2} C_\rho \left(\frac{\Lambda_\rho^2 - m_\rho^2}{\Lambda_\rho^2 - q^2} \right)^2 + g' \right], \quad (26)$$

where $\frac{f^2}{4\pi} = 0.8$, $\Lambda_\pi = 1.3$ GeV, $C_\rho = 2$, $\Lambda_\rho = 2.5$ GeV, m_π and m_ρ are the pion and rho meson masses, and g' is the Landau-Migdal parameter taken to be 0.7 which has been used quite successfully to explain weak processes in nuclei [35, 50, 51, 57]. However, in some recent works, the Valencia group [41, 44, 64] has used the value of $g' = 0.63$. We have, therefore, studied the dependence of g' on the total cross section as well as lepton energy and angular distributions by varying g' in the range of 0.6 to 0.7.

The effect of the Δ degrees of freedom in the nuclear medium is included in the calculation of the RPA response by considering the effect of ph- Δ h and Δ h- Δ h excitations. This is done by replacing $U_N \rightarrow U'_N = U_N + U_\Delta$, where U_Δ is the Lindhard function for the Δ h excitation in the nuclear medium. The expressions for U_N and U_Δ are taken from Ref.[65]. The different couplings of N and Δ are incorporated in U_N and U_Δ and then the same interaction strengths (V_l and V_t) are used to calculate the RPA response.

With the incorporation of these nuclear medium effects the expression for the total scattering cross section $\sigma(E_\nu)$ is given by Eq.(24) with $J^{\mu\nu}$ replaced by $J_{RPA}^{\mu\nu}$ (defined in Eq. (25)) i.e.

$$\sigma(E_\nu) = -2G_F^2 \cos^2 \theta_c \int_{r_{min}}^{r_{max}} r^2 dr \int_{k'_{min}}^{k'_{max}} k' dk' \int_{Q^2_{min}}^{Q^2_{max}} dQ^2 \frac{1}{E_\nu^2 E_l} L_{\mu\nu} J_{RPA}^{\mu\nu} Im U_N (q_0^{eff}(r) - V_c(r)), \quad (27)$$

where $J_{RPA}^{\mu\nu}$ is the hadronic tensor with its various components modified due to long range correlation effects treated in RPA as it is shown in Eq.(25) for the leading term proportional to F_A^2 . The explicit expressions for $J_{RPA}^{\mu\nu}$ is given in the Ref.[54].

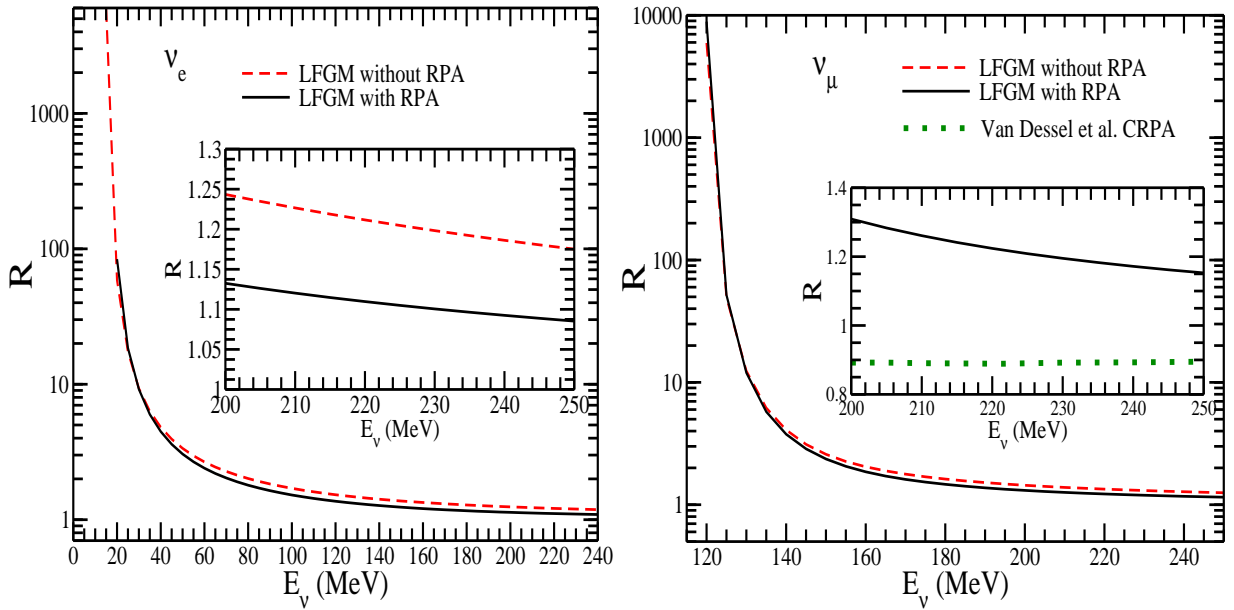


FIG. 6. Ratio, $R = \frac{\sigma_{\nu_l}^{40Ar}}{\sigma_{\nu_l}^{12C}}$ vs E_ν for ν_e (left panel) and ν_μ (right panel). Solid(dashed) line represents the results obtained using LFGM with(without) RPA. In the inset of ν_e case(left panel), the results of the ratio are obtained without(dashed line) and with(solid line) RPA. In the inset of ν_μ case(right panel), the results are compared with the results of Van Dessel et al. [68] in CRPA(dotted line).

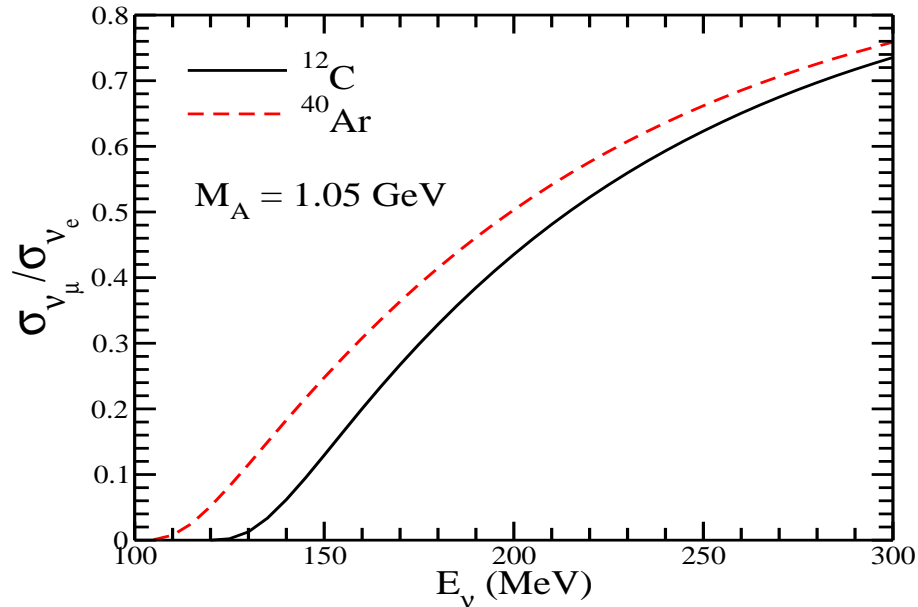


FIG. 7. Ratio of ν_μ to ν_e scattering cross sections $\frac{\sigma_{\nu_\mu}}{\sigma_{\nu_e}}$ vs E_ν for ^{12}C (solid line) and ^{40}Ar (dashed line) in the LFGM with RPA.

III. RESULTS AND DISCUSSION

For the numerical calculations, we have used Eq. 24 to obtain the results for the charged current ν_e and ν_μ scattering cross sections on the nuclear targets in the local Fermi gas model(LFGM) with the inclusion of Fermi momentum and Pauli blocking, and Eq. 27 when RPA effects are also included. Furthermore, we have taken Coulomb distortion effect on the outgoing charged lepton in both cases using EMA with the Coulomb potential given in Eq. 23.

In Fig. 3, we present the results of $\nu_l(l=e, \mu)$ induced charged lepton production cross sections σ vs E_{ν_l} in ^{12}C and

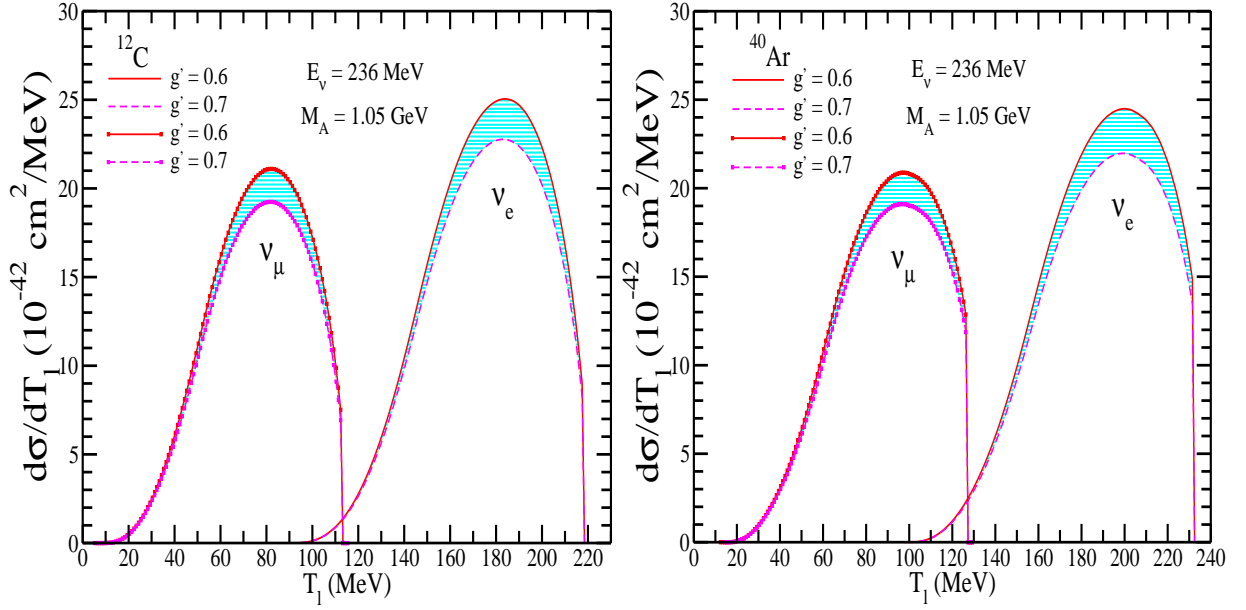


FIG. 8. $\frac{d\sigma}{dT_l}$ vs T_l for ν_l induced processes on ^{12}C (left panel) and ^{40}Ar (right panel) nuclear targets at $E_\nu = 236$ MeV. The results are obtained using LFGM with RPA. The variation of g' from 0.6 to 0.7 is represented by the band. The curves on the left (right) side of each panel represent the results for μ^- (e^-) kinetic energy distribution induced by ν_μ (ν_e) scattering.

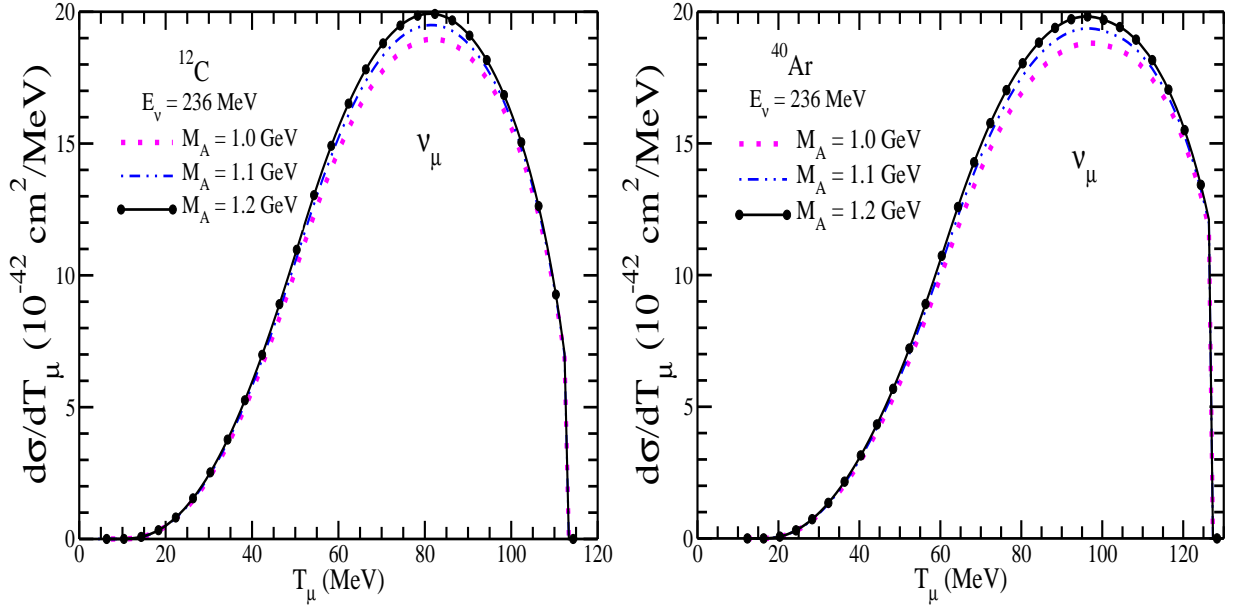


FIG. 9. $\frac{d\sigma}{dT_\mu}$ vs T_μ for ν_μ induced processes on ^{12}C (left panel) and ^{40}Ar (right panel) nuclear targets at $E_\nu = 236$ MeV. The results are obtained using LFGM with RPA for the different values of M_A viz. $M_A = 1.0$ GeV (dotted line), 1.1 GeV (dash double-dotted line) and 1.2 GeV (circle), respectively.

^{40}Ar , respectively. We find a large reduction in the cross section due to the nuclear medium effects. For example, in the case of ν_e scattering on ^{12}C (^{40}Ar) nuclear targets, when the cross section is obtained using the LFGM without RPA effects, the reduction in the cross section from the free nucleon case (not shown here) is $\sim 50\%$ (35%) at $E_{\nu_e} = 150$ MeV, $\sim 38\%$ (20%) at $E_{\nu_e} = 200$ MeV and $\sim 30\%$ (15%) at $E_{\nu_e} = 236$ MeV. When the RPA effects are also taken into account there is a further reduction in the cross section which is about $\sim 48\%$ (53%) at $E_{\nu_e} = 150$ MeV, $\sim 45\%$ (50%) at $E_{\nu_e} = 200$ MeV and $\sim 42\%$ (47%) at $E_{\nu_e} = 236$ MeV. In the case of ν_μ scattering, this reduction is $\sim 85\%$ (65%) at $E_{\nu_\mu} = 150$ MeV, $\sim 60\%$ (43%) at $E_{\nu_\mu} = 200$ MeV and $\sim 47\%$ (30%) at $E_{\nu_\mu} = 236$ MeV without the RPA correlation

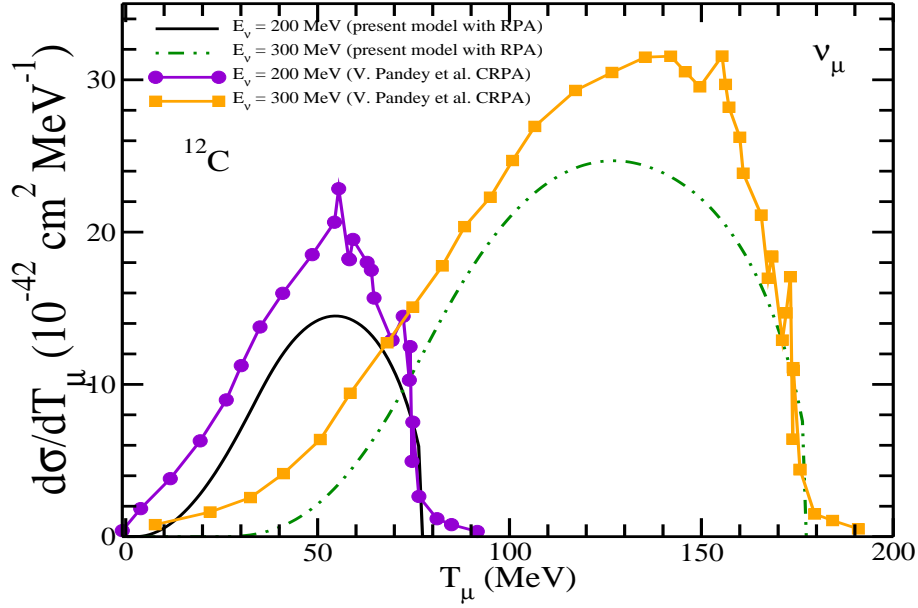


FIG. 10. Kinetic energy distribution, $\frac{d\sigma}{dT_\mu}$ vs T_μ for ν_μ induced process on ^{12}C nuclear target. The results of LFGM with RPA are represented by solid line at $E_\nu = 200$ MeV and by dash double-dotted line at $E_\nu = 300$ MeV. The results obtained from the Ref. [71] at $E_\nu = 200$ MeV(circle) and $E_\nu = 300$ MeV(square) are also presented in the figure.

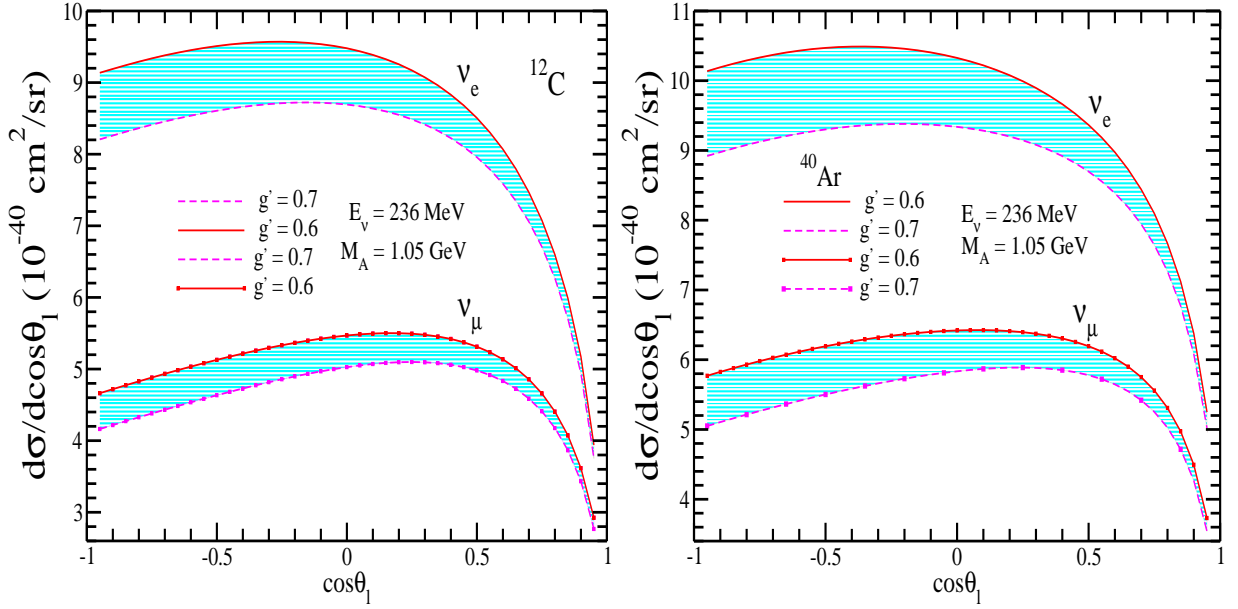


FIG. 11. $\frac{d\sigma}{d\cos\theta_l}$ vs $\cos\theta_l$ for ν_l induced process on ^{12}C (left panel) and ^{40}Ar (right panel) at $E_\nu=236\text{MeV}$, obtained by using LFGM with RPA. The variation of g' from 0.6 to 0.7 is represented by the band. Solid and dashed lines present the results of ν_e scattering and dotted and dash double-dotted lines represent the results of ν_μ scattering.

and a further reduction of $\sim 55\%$ (60%) at $E_{\nu_\mu} = 150$ MeV, $\sim 50\%$ (55%) at $E_{\nu_\mu} = 200$ MeV and $\sim 45\%$ (50%) at $E_{\nu_\mu} = 236$ MeV, when RPA effects are included. We have also shown in these figures, the dependence of the cross section on g' , the Landau-Migdal parameter, used in Eq. (26) by varying the value of g' in the range 0.6-0.7. The bands shown in the figures correspond to the change in the cross section due to the variation of g' in this range. We find that with $g' = 0.7$ the cross section in $^{12}\text{C}/^{40}\text{Ar}$ decreases by about 10% for $\nu_l(l = e, \mu)$ scattering at 236 MeV from the results obtained with $g' = 0.6$.

In Figs. 4 and 5, we have compared the present results in $\nu_e - ^{12}\text{C}$ with the results of NuWro generator [25], Volpe

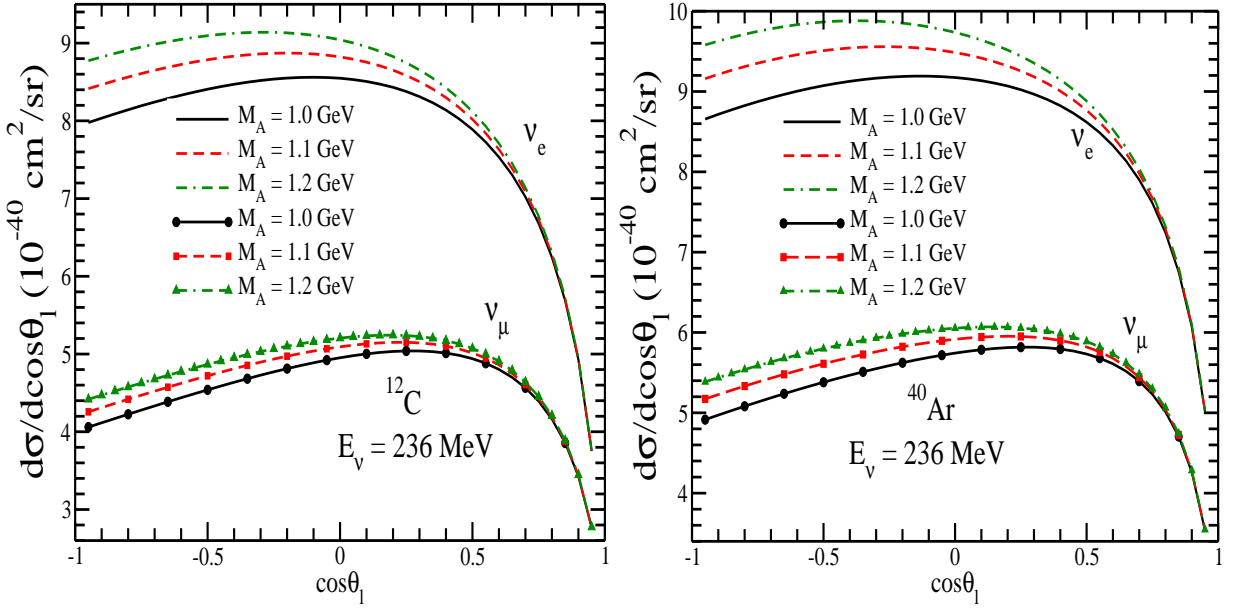


FIG. 12. $\frac{d\sigma}{d\cos\theta_l}$ vs $\cos\theta_l$ for ν_e (top curves) and ν_μ (bottom curves) induced processes on ^{12}C (left panel) and ^{40}Ar (right panel) nuclear targets at $E_\nu = 236$ MeV, obtained by using LFGM with RPA for the different values of M_A viz. $M_A = 1.0$ GeV (circle), 1.1 GeV (dash double-dotted line) and 1.2 GeV (dotted line).

et al. [36] in Random Phase Approximation, Kolbe et al. [38] in Continuum Random Phase Approximation, Paar et al. [42] in Relativistic Quasiparticle Random Phase Approximation, Samana et al. [66] in Projected Quasiparticle Random Phase Approximation-S6, and Smith and Moniz [67] in the relativistic Fermi gas model. In the case of $\nu_\mu - ^{12}\text{C}$, $\nu_e - ^{40}\text{Ar}$ and $\nu_\mu - ^{40}\text{Ar}$ induced processes, the cross section results are compared with the results of Smith and Moniz [67] and NuWro generator [20, 25] in which the nucleon spectral function of Benhar et al. [30] has been used.

In the preliminary simulation studies for determining the neutrino oscillation parameters Spitz et al. [19, 20] have used NuWro [25] prediction of 1.3×10^{-38} cm² per neutron for the total cross section for $\nu_\mu - ^{12}\text{C}$ and $\nu_\mu - ^{40}\text{Ar}$ scattering at $E_\nu = 236$ MeV. and the same value has also been used by Axani et al. [18] for the $\nu_\mu - ^{12}\text{C}$ cross section. In view of this we have studied the ratio $R = \frac{\sigma_{^{40}\text{Ar}}}{\sigma_{^{12}\text{C}}}$ as a function of E_ν . In Fig. 6, we have shown the results for R obtained using the present model with and without RPA effects for the ν_e and ν_μ induced processes and also made a comparison with the recent results reported by Van Dessel et al. [68] in CRPA for the ν_μ induced process.

The measurement of neutrino-nucleus cross section induced by ν_μ and ν_e and the ν_μ/ν_e cross section ratio is an important quantity in the analysis of $\nu_\mu \rightarrow \nu_e$ oscillations in the appearance channel. This ratio also provides an experimental validation of the theoretical calculations of the various effects arising due to the lepton mass dependent terms in the standard model specially the pseudoscalar form factors and the second class currents [54, 69] and could provide possible evidence of muon-electron non-universality. Moreover, this ratio is also a key parameter in improving the sensitivity of measuring the CP violation phase δ_{CP} in the future experiments on neutrino oscillations [70]. We have plotted in Fig. 7, the ratio of ν_μ/ν_e cross section as a function of energy in the low energy region relevant for the experiments with KDAR neutrinos.

In Fig. 8, we have presented the results of $\frac{d\sigma}{dT_l}$ vs T_l ($l = e, \mu$), for ν_e and ν_μ induced processes in ^{12}C (left panel) and ^{40}Ar (right panel) nuclear targets at $E_\nu = 236$ MeV. The results are shown by varying g' in the range 0.6 to 0.7 using $M_A = 1.05$ GeV.

In Fig. 9, we have presented the results for $\frac{d\sigma}{dT_\mu}$ vs T_μ in ^{12}C and ^{40}Ar nuclear targets at $E_\nu = 236$ MeV by varying M_A in the range of 1 - 1.2 GeV. We observe that there is very little sensitivity on M_A in the case of kinetic energy distribution which is around 5% when we vary the value of M_A by 20%.

In Fig. 10, we show the energy distribution $\frac{d\sigma}{dT_\mu}$ vs T_μ at the two different neutrino energies, viz., $E_{\nu_\mu} = 200$ MeV and $E_{\nu_\mu} = 300$ MeV on ^{12}C calculated in the present model and compare them with the results of Pandey et al. [71]. We see that there is wide variation in the energy distribution of muons predicted in these two models.

In Fig. 11, we have presented the results of the angular distribution $\frac{d\sigma}{d\cos\theta_l}$ vs $\cos\theta_l$ for ν_e and ν_μ induced processes in ^{12}C (left panel) and ^{40}Ar (right panel) nuclear targets at $E_\nu = 236$ MeV. The results are obtained by varying g' in

the range 0.6 to 0.7 using $M_A=1.05\text{GeV}$.

In Fig. 12, we have presented the results for ν_e and ν_μ induced processes in ^{12}C and ^{40}Ar nuclear targets at $E_\nu = 236\text{ MeV}$ by varying M_A in the range of 1 - 1.2GeV. We observe that there is some sensitivity on M_A in the case of angular distribution specially at the backward angles corresponding to higher Q^2 .

IV. SUMMARY AND CONCLUSIONS

We have presented a theoretical description of the inclusive quasielastic scattering for ν_e and ν_μ scattering induced by the weak charged current on ^{12}C and ^{40}Ar relevant for the future experiments planned to be done using KDAR neutrinos. These KDAR neutrinos are monoenergetic with $E_{\nu_\mu}=236\text{MeV}$. The neutrino oscillation experiments in the $\nu_\mu \rightarrow \nu_\mu$ and $\nu_\mu \rightarrow \nu_e$ channels have background from the KDAR neutrinos from the $K_{\mu 3}$ and $K_{e 3}$ decay modes with the continuous energy spectrum of the muon neutrinos with $E_{\nu_\mu} \leq 215\text{MeV}$ and the electron neutrinos with $E_{\nu_e} \leq 235\text{MeV}$. We have therefore studied the nuclear medium effects in the neutrino-nucleus cross sections in the energy region of $E_{\nu_i} \leq 300\text{MeV}$ for QE scattering of ν_e and ν_μ from ^{12}C and ^{40}Ar nuclear targets proposed to be used in the future experiments planned at the JPARC and Fermilab facilities with liquid scintillator(LS) and LArTPC detectors.

The calculations have been done in a microscopic model of nucleus which takes into account the effect of the Fermi motion, binding energy and long range nucleon-nucleon correlations through RPA. The method has been earlier applied successfully to reproduce the low energy neutrino-nucleus cross sections observed in LSND, KARMEN and LAMPF experiments. The effect of Pauli blocking and RPA correlations is to drastically reduce the cross sections over the free nucleon case. In the energy region of $E_\nu = 150 - 250\text{MeV}$, the overall reduction due to Pauli blocking and RPA correlations in ^{12}C (^{40}Ar) varies from the range of 70%(75%) to 55%(53%) in the case of ν_e -nucleus scattering and 95%(85%) to 68%(63%) in the case of ν_μ -nucleus scattering. There is an uncertainty of about 10% due to the Landau-Migdal parameter used in the treatment of RPA correlations. The results have been compared with the results of the other calculations in the literature. The cross section obtained using the present model with RPA effect is around 50% smaller than the results of the Relativistic Fermi gas model(RFGM) of Smith and Moniz [67]. The different treatment of nucleon-nucleon correlations in the various approaches discussed in section-III results in an uncertainty of about 25% in the cross sections at $E_{\nu_\mu}=236\text{MeV}$.

We have also presented the results for the energy and angular distributions for e^- and μ^- produced in these reactions for a fixed neutrino energy of $E_\nu=236\text{MeV}$. A comparison with the recent results of Pandey et al. [71] shows that the differences in the prediction of these two models are significant in the case of the energy distributions of the muons. An experimental observation of the total cross sections and the differential cross sections in the forthcoming experiments will be able to discriminate between various models of treating the nuclear medium effects in the neutrino-nucleus scattering at low energies.

-
- [1] C. Patrignani *et al.* [Particle Data Group], *Chin. Phys. C* **40**, 100001 (2016).
 - [2] T. Katori and M. Martini, arXiv:1611.07770 [hep-ph].
 - [3] L. Alvarez-Ruso, Y. Hayato and J. Nieves, *New J. Phys.* **16**, 075015 (2014).
 - [4] K. N. Abazajian *et al.*, arXiv:1204.5379 [hep-ph].
 - [5] K. Abe *et al.* [T2K Collaboration], K. Abe *et al.* [T2K Collaboration], arXiv:1706.04257 [hep-ex]. *Phys. Rev. Lett.* **112**, 061802 (2014).
 - [6] M. Antonello *et al.* [MicroBooNE and LAr1-ND and ICARUS-WA104 Collaborations], arXiv:1503.01520 [physics.ins-det].
 - [7] Y. T. Tsai [MicroBooNE Collaboration], arXiv:1705.07800 [hep-ex].
 - [8] R. Acciarri *et al.* [MicroBooNE Collaboration], *JINST* **12**, no. 02, P02017 (2017).
 - [9] Marcos Dracos, *Physics Procedia* 61, 459 (2015).
 - [10] E. Baussan *et al.* [ESSnuSB Collaboration], *Nucl. Phys. B* **885**, 127 (2014)
 - [11] W. G. S. Vinning and A. Blake, arXiv:1705.06561 [hep-ph].
 - [12] J. Cao *et al.*, *Phys. Rev. ST Accel. Beams* **17**, 090101 (2014)
 - [13] D. Adey, R. Bayes, A. Bross and P. Snopok, *Ann. Rev. Nucl. Part. Sci.* **65**, 145 (2015).
 - [14] A. Liu, A. Bross, D. Neuffer and S. Y. Lee, PAC-2013-TUPBA18, FERMILAB-CONF-13-451-APC.
 - [15] S. Ajimura *et al.*, arXiv:1705.08629 [physics.ins-det].
 - [16] M. Harada *et al.*, arXiv:1601.01046 [physics.ins-det].
 - [17] M. Harada *et al.*, arXiv:1502.02255 [physics.ins-det].
 - [18] S. Axani, G. Collin, J. Conrad, M. Shaevitz, J. Spitz and T. Wongjirad, *Phys. Rev. D* **92**, 092010 (2015).
 - [19] J. Spitz, *Phys. Rev. D* **89**, 073007 (2014).
 - [20] J. Spitz, *Phys. Rev. D* **85**, 093020 (2012).
 - [21] J. Grange Private communication.

- [22] C. Rott, S. In, J. Kumar and D. Yaylali, JCAP **1701**, 016 (2017).
- [23] S. Agostinelli *et al.* [GEANT4 Collaboration], Nucl. Instrum. Meth. A **506**, 250 (2003).
- [24] N. V. Mokhov *et al.*, Radiat. Prot. Dosim. **116**, 99 (2005)
- [25] C. Juszczak, “Running NuWro,” Acta Phys. Polon. B **40**, 2507 (2009); <http://borg.ift.uni.wroc.pl/nuwro/>
- [26] C. Andreopoulos *et al.*, Nucl. Instrum. Meth. A **614**, 87 (2010).
- [27] M. Martini, M. Ericson and G. Chanfray, Phys. Rev. C **84**, 055502 (2011).
- [28] M. Martini, M. Ericson, G. Chanfray and J. Marteau, Phys. Rev. C **80**, 065501 (2009).
- [29] J. Nieves, F. Sanchez, I. Ruiz Simo and M. J. Vicente Vacas, Phys. Rev. D **85**, 113008 (2012).
- [30] O. Benhar, N. Farina, H. Nakamura, M. Sakuda and R. Seki, Phys. Rev. D **72**, 053005 (2005)
- [31] M. Martini, M. Ericson and G. Chanfray, Phys. Rev. D **87**, 013009 (2013).
- [32] T. S. Kosmas and E. Oset, Phys. Rev. C **53**, 1409 (1996).
- [33] J. Engel, E. Kolbe, K. Langanke and P. Vogel, Phys. Rev. C **54**, 2740 (1996).
- [34] N. Auerbach, N. Van Giai and O. K. Vorov, Phys. Rev. C **56**, R2368 (1997).
- [35] S. K. Singh, N. C. Mukhopadhyay and E. Oset, Phys. Rev. C **57**, 2687 (1998).
- [36] C. Volpe, N. Auerbach, G. Colo, T. Suzuki and N. Van Giai, Phys. Rev. C **62**, 015501 (2000).
- [37] A. C. Hayes and I. S. Towner, Phys. Rev. C **61**, 044603 (2000).
- [38] E. Kolbe, K. Langanke and P. Vogel, Nucl. Phys. A **652**, 91 (1999).
- [39] N. Auerbach and B. A. Brown, Phys. Rev. C **65**, 024322 (2002).
- [40] E. Kolbe, K. Langanke, G. Martinez-Pinedo and P. Vogel, J. Phys. G **29**, 2569 (2003).
- [41] J. Nieves, J. E. Amaro and M. Valverde, Phys. Rev. C **70**, 055503 (2004).
- [42] N. Paar, D. Vretenar, T. Marketin and P. Ring, Phys. Rev. C **77**, 024608 (2008).
- [43] N. Paar, D. Vretenar and P. Ring, J. Phys. G **35**, 014058 (2008).
- [44] J. Nieves and J. E. Sobczyk, Annals Phys. **383**, 455 (2017).
- [45] M. Albert *et al.* [LSND Collaboration], Phys. Rev. C **51**, 1065 (1995).
- [46] C. Athanassopoulos *et al.* [LSND Collaboration], Phys. Rev. C **56**, 2806 (1997).
- [47] L. B. Auerbach *et al.* [LSND Collaboration], Phys. Rev. C **66**, 015501 (2002).
- [48] M. Sajjad Athar and S. K. Singh, Phys. Lett. B **591**, 69 (2004).
- [49] M. Sajjad Athar, S. Ahmad and S. K. Singh, Phys. Rev. C **71**, 045501 (2005).
- [50] M. Sajjad Athar, S. Ahmad and S. K. Singh, Nucl. Phys. A **764**, 551 (2006).
- [51] S. Chauhan, M. Sajjad Athar and S. K. Singh, Int. J. Mod. Phys. E **26**, 1750047 (2017).
- [52] R. Bradford, A. Bodek, H. S. Budd and J. Arrington, Nucl. Phys. Proc. Suppl. **159**, 127 (2006).
- [53] C. H. Llewellyn Smith, Phys. Rept. **3**, 261 (1972).
- [54] F. Akbar *et al.*, Int. J. Mod. Phys. E **24**, 1550079 (2015).
- [55] C. W. de Jager *et al.*, Atomic data and Nuclear data tables, **14**, 479 (1974); H. de Vries *et al.*, Atomic data and Nuclear data tables, **36**, 495 (1987).
- [56] C. Garcia-Recio, J. Nieves and E. Oset, Nucl. Phys. A **547**, 473 (1992).
- [57] S. K. Singh and E. Oset, Phys. Rev. C **48**, 1246 (1993).
- [58] Quantum Theory of Many-Particle Systems by Alexander L. Fetter and John Dirk Walecka, McGraw-Hill, New York, 1971
- [59] C. Itzykson and J.-B. Zuber, Quantum Field Theory, McGraw-Hill, 1980.
- [60] J. Engel, Phys. Rev. C **57**, 2004 (1998).
- [61] K. S. Kim, L. E. Wright, Y. Jin and D. W. Kosik, Phys. Rev. C **54**, 2515 (1996).
- [62] M. Traini, Nucl. Phys. A **694**, 325 (2001).
- [63] A. Aste, C. von Arx, and D. Trautmann, Eur. Phys. J. A **26** 167 (2005).
- [64] M. Valverde, J. E. Amaro and J. Nieves, Phys. Lett. B **638**, 325 (2006).
- [65] E. Oset, D. Strottman, H. Toki and J. Navarro, Phys. Rev. C **48**, 2395 (1993); E. Oset, P. Fernandez de Cordoba, L. L. Salcedo and R. Brockmann, Phys. Rept. **188**, 79 (1990).
- [66] A. R. Samana, F. Krmpotic, N. Paar and C. A. Bertulani, J. Phys. Conf. Ser. **312**, 072009 (2011).
- [67] R. A. Smith and E. J. Moniz, Nucl. Phys. B **43**, 605 (1972).
- [68] N. Van Dessel, N. Jachowicz, R. Gonzalez-Jimnez, V. Pandey and T. Van Cuyck, arXiv:1704.07817 [nucl-th].
- [69] M. Day and K. S. McFarland, Phys. Rev. D **86**, 053003 (2012).
- [70] P. Huber, M. Mezzetto and T. Schwetz, JHEP **0803**, 021 (2008).
- [71] V. Pandey, N. Jachowicz, T. Van Cuyck, J. Ryckebusch and M. Martini, Phys. Rev. C **92**, 024606 (2015); N. Jachowicz, V. Pandey, M. Martini, R. Gonzalez-Jimnez, T. Van Cuyck and N. Van Dessel, JPS Conf. Proc. **12**, 010018 (2016).